Indian Geotech J
https://doi.org/10.1007/s40098-024-01006-4

ORIGINAL PAPER

Numerical Investigation Study on the Performance of Strip Footing Under Eccentric Loading Condition Embedded in Nonhomogeneous Clay Soils

Nassima Zatar[1,2] · **Messaoud Baazouzi**[1,3] · **Alaoua Bouaicha**[1,4] · **Khawla Boudiaf**[1,5] · **Abdallah Zatar**[1] · **Abdelhak Mabrouki**[1]

Received: 2 March 2024 / Accepted: 11 June 2024

Abstract This study investigates the undrained bearing capacity and failure mechanisms of strip footings embedded in non-homogeneous clay layers subjected to eccentric vertical loads, addressing the stability concerns associated with eccentric loading conditions commonly encountered in the foundations of buildings, retaining walls, and bridge abutments. The study examines the influence of critical factors, including eccentric loading, interface effects, and depth ratio (D/B), on the bearing capacity of both the surface and embedded strip footings. Employing elastoplastic finite element analyses of the Tresca soil model, the study compares its results using existing literature to evaluate the impact of these factors on the undrained bearing capacity of perfectly rough and smooth strip footings. The results demonstrate that these factors significantly influence the undrained bearing capacity, highlighting the importance of considering these variables in geotechnical design.

Keywords Bearing capacity · Embedded shallow foundation · Failure mechanism · Interface nonhomogeneous

✉ Messaoud Baazouzi
m.baazouzi@univ-khenchela.dz

Nassima Zatar
n.zatar@univ-batna2.dz

Alaoua Bouaicha
alaoua.bouaicha@univ-biskra.dz

Khawla Boudiaf
boudiaf.khoula@univ-khenchela.dz

Abdallah Zatar
abdallah.zatar@univ-biskra.dz

Abdelhak Mabrouki
a.mabrouki@univ-biskra.dz

[1] Civil Engineering Research Laboratory LRGC, Biskra University, 07000 Biskra, Algeria

[2] Civil Eng Department, Faculty of Technology, University Mostafa Benboulaid, 05078 Batna, Algeria

[3] Civil Eng Department, Faculty of Sciences and Technology, University Abbes Laghrour, 40000 Khenchela, Algeria

[4] Scientific and Technical Research Center on Arid Regions CRSTRA, Campus of Mohamed Khider University, 07000 Biskra, Algeria

[5] Civil Eng Department, Faculty of Civil Engineering, University Houari Boumediene, 16111 Alger, Algeria

List of Symbols

k	Strength non-homogeneity rate
h/B	Soil layer thickness-to-footing width ratio
D/B	Footing embedment ratio
e/B	Load eccentricity ratio
B/B_0	Normalized failure zone width
kB/c_0	Non-homogeneity factor
N_c	Vertical bearing capacity factor
c_u	Undrained shear strength varies linearly with depth
B	Width of the footing
c_0	Undrained shear strength at the surface level
E_u	Young modulus
E_0	Young's modulus at the soil surface
σ_n	Normal stresses
FEA	Finite element analysis
DLO	Discontinuity layout optimization
RPFEM	Rigid plastic finite element method

Introduction

The presence of shallow, rigid subsurface strata significantly influences the behavior of strip footings subjected

Published online: 19 June 2024

to vertical loading. Traditionally, the assessment of foundation-bearing capacity relies on Terzaghi's [1] superposition equation. However, in reality, soils are naturally stratified into layers [2]. Furthermore, natural soil is not merely a binary composition of sand or clay; it represents a complex amalgamation with varying levels of adhesiveness and resistance [3, 4]. Researchers have diligently investigated how footings interact with diverse soil types, including sandy, clayey, and mixed compositions, aiming to determine their ultimate load-bearing capacity. Notably, construction sites, often partially saturated or composed of weathered soft rock, typically fall within the category of frictional-cohesive soil. Despite their prevalence, research on such types of soils remains limited. Specifically, using bearing capacity factors aligned with Terzaghi's theory remains elusive for this nonhomogeneous soil type.

In practical engineering scenarios, foundation systems experience loads encompassing self-weight, inclined or eccentric dead loads, operational forces, and environmental pressures. This intricate loading scenario is typically represented by a three-dimensional yield envelope, defining the ultimate capacity under multiaxial loading conditions through the combined vertical (V), horizontal (H), and moment (M) capacities. Notably, offshore foundations confront substantial cyclic loads from harsh environmental conditions—such as wind, waves, and currents. Consequently, offshore design mandates meticulous consideration of cyclic loading effects on bearing capacity [5]. The presence of weak and rigid soils surrounding the foundation emerges as a critical concern for engineers, as it can lead to a substantial reduction in foundation capacity and a pronounced accumulation of displacement, including repeated foundation rotation. Drawing upon extensive research into the bearing behavior of strip foundations under eccentric loads, various investigations have scrutinized and assessed the ultimate limit state of such foundations under eccentric loading conditions [6, 7]. In addition to the effective footing width method, two alternative approaches have surfaced: the methodology proposed by Meyerhof [8] and the conventional analytical technique described by Uzuner [9].

In the context of evaluating Meyerhof's [8] proposed method for eccentrically loaded foundations, a rigid strip footing underwent a systematic series of load applications to ascertain its bearing capacity under eccentric vertical loading conditions. According to the proposition of Meyerhof, the effective footing width is $B = B + 2e$. B represents the footing width and the eccentricity (e) between the loading point and the center of the footing.

This effective width approach finds common application in footing design. Notably, the conventional analysis method, depicted in Fig. 1, introduces additional assumptions to delineate the distribution of base normal stresses under eccentric vertical loads. Specifically, a linear stress distribution is valid within three distinct eccentricity ranges ($e/B < 1/6$, $e/B = 1/6$, $e/B > 1/6$), where σ_n (max) and σ_n (min) are the maximum normal stress and the minimum normal stress, respectively. Importantly, when tensile stresses manifest at significant eccentricities ($e/B > 1/6$), the footing base disengages from the soil. Notably, a comprehensive systematic analysis of these methods across varying soil conditions remains absent, leaving their applicability unresolved. Consequently, the ultimate bearing capacity of the footing significantly hinges upon the soil type and the applied loads.

The bearing capacity of eccentrically loaded footings on sandy soils can be effectively determined using limit analysis, a powerful geotechnical tool. This approach has found successful application across diverse footing configurations, encompassing embedded strip footings as explored by (Bransby and Randolph. [11]), embedded circular foundations (Vulpe et al. [12]), and skirted circular footings featuring a deformable soil plug, as studied by (Gourvence et al. [13]). These studies highlighted the significant influence of the embedment ratio on both the ultimate uniaxial capacity and the shape of the yield surface for embedded foundations. Furthermore, the influence of soil strength heterogeneity on these critical aspects has been prominently highlighted.

Bienen et al. [14] investigated the soil failure mechanisms associated with a hybrid foundation subjected to combined vertical (V), horizontal (H), and moment (M) loading conditions. The research focused on optimizing the amount of steel in hybrid foundations to enhance their resistance to

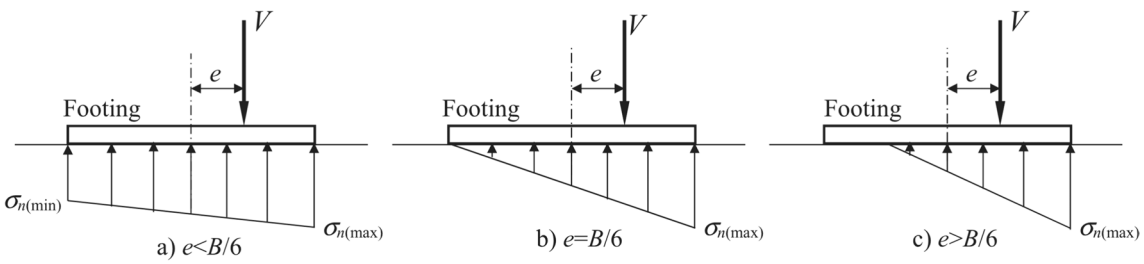

Fig. 1 Distribution of base normal stresses under different eccentricities in customary analysis method [10]

horizontal and moment loads. They found that using steel efficiently in these foundations improves their resistance to sideways and moment forces. The longer hybrid foundation also strengthens them, especially against sideways pressure. Unlike more straightforward foundations, these stilted ones have different ways of failing due to their complex shape.

Fu et al. [15] conducted centrifuge tests to investigate the influence of preloading on the bearing capacity of skirted circular foundations. They measured how much stronger these foundations became after pre-loading the soil. They discovered that applying some pressure before the main load increases their ability to support weight. In subsequent work, Fu et al. [16] analyzed the failure mechanisms and load distribution of these foundations, considering variations in soil strength under specific conditions. They also devised a new way to predict how much weight these foundations can handle in different directions. This method helps engineers determine the strength of such foundations based on soil properties and their shape.

Khitas et al. [6] investigated how the connection between the soil and the foundation, particularly its ability to resist pulling forces, affects the load-bearing capacity of long, narrow foundations. Their analysis showed that the pressure spread remains consistent regardless of where the load is placed, suggesting a predictable relationship between load placement and pressure distribution. However, Pham et al. [17] employed limit analysis to investigate the distribution of contact normal stresses (σ_n) on a footing base subjected to vertical loads and found that the pressure distribution under vertical loads forms a triangular pattern, which changes depending on where the load is placed. This highlights the importance of load placement on how pressure is distributed under vertical loads.

Hentati et al. [18] undertook a rigorous exploration of the impact of spatial variability in undrained soils on the response of strip foundations subjected to combined horizontal (H) and moment (M) loadings. Their investigation employed an advanced methodology that seamlessly integrated finite element analysis (FEA), random field theory, and Monte Carlo simulations to account for uncertainties and spatial variability in soil properties. This comprehensive approach allowed for thoroughly examining system behavior across diverse conditions, accounting for inherent uncertainties and spatial irregularities. Notably, the researchers modeled the undrained shear strength of the soil beneath the foundation as a lognormally distributed random field.

Zheng et al. [19] employed discontinuity layout optimization (DLO) to ascertain the bearing capacity and failure mechanisms of obliquely loaded footings situated above infinite-depth sand, leading to the development of a simplified model for predicting bearing capacity. Meanwhile, Pham et al. [10] delved into the ultimate bearing capacity of c-φ soils under eccentric and inclined loads using the rigid plastic finite element method (RPFEM). By leveraging the Drucker and Prager [20] yield criterion, their study extended the applicability of the rigid plastic constitutive equation to soil types with intricate material properties, enabling a more realistic analysis of soil behavior under varying loading conditions.

This research employed finite element analysis, using OptumG2 [21] to assess the bearing capacity factors and failure envelopes of strip footings embedded in non-homogeneous clay layers under eccentric loading conditions. The study considers various configurations, including both interface and embedded footings, while investigating the influence of strength non-homogeneity rate (k), soil layer thickness-to-footing width ratio (h/B), and footing embedment ratio (D/B) in relation to load eccentricity (e/B).

Problem Definition

The problem studied considers surface and embedded strip footings under eccentric loads on a nonhomogeneous clay layer at different depths below the strip footing.

The undrained bearing capacity of strip footing is calculated as follows:

$$q_u = c_0 \cdot N_c \tag{1}$$

where c_0 is the undrained shear strength at the surface (Fig. 2), and N_c is the vertical bearing capacity factor function of c_u and the rigid base depth. c_u is expressed as:

$$c_u = c_0 + k \cdot z \tag{2}$$

where c_u represents the undrained shear strength, which varies linearly with depth, z, while k represents the gradient of cohesion with depth, z.

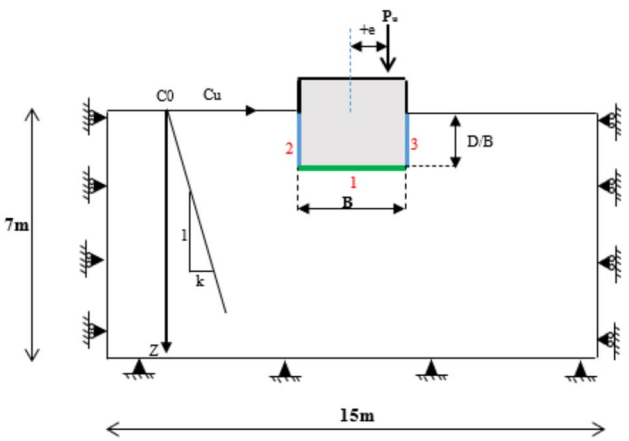

Fig. 2 Problem definition

Non-homogeneity is represented by the non-dimensional ratio $j = k{\cdot}B/c_0$, where B is the width of the footing, and layer thickness is defined by the non-dimensional ratio h/B, which is the ratio of soil layer thickness to footing width. Matar and Salencon [22] provide a precise definition of bearing capacity as:

$$q_u = p + u_c c_0 \left(N_{rc} + \frac{1}{4}\frac{kB}{c_0} \right) \tag{3}$$

The Eq. (3) incorporates the uniform surcharge pressure (p) and dimensionless coefficients u_c and N_c. These coefficients depend on the non-homogeneity factor (k) and the soil layer thickness-to-footing width ratio (h/B). Values for u_c and N_c can be obtained directly or through interpolating from the provided charts.

The soil behavior is modeled using the Tresca yield criterion, which assumes a perfectly plastic material with equal shear strength in tension and compression. The model incorporates a non-homogeneous undrained shear strength profile, reflecting increased strength with depth. At the surface level, the undrained shear strength is $c_0 = 50$ kPa. The variable k symbolizes the strength gradient. The non-dimensional embedment depth (D/B) remains within the range of 0–2.5 in all the analyses.

Finite Element Limit Analysis

The commercial software application OPTUM G2 [21] has proven to be a highly effective tool for researchers who analyze the two-dimensional behavior of structures made from materials such as soil or rock. This program simulates structures that experience plastic flow once they reach their yield limits. Many researchers have utilized OPTUM G2 [21] to perform analyses of the bearing capacity of both strip and circular footings, slope stability [23, 24], making it a widely trusted choice for such investigations.

The unconsolidated bearing capacity of strip footings with rough surfaces was thoroughly evaluated in this study, considering the effects of eccentric loads on non-uniform clay. The strength gradient (k) was varied across various values, including 0, 1, 3, 5, 10, 20, 50, and 100. The analysis encompassed a non-dimensional embedment depth (D/B) range of 0–2.5.

Figure 3 shows a typical finite element mesh used to analyze a footing with a width B of 2 m and a depth of embedment D/B of 1 m. Adaptive meshing avoids the size effect, while shear dissipation controls the size effect. To ensure high levels of accuracy, the software manual recommends three adaptive iterations. A size consists of 2000 elements. Since there is no loading symmetry, the entire soil domain ($15B * 7B$) is considered. Larger mesh sizes do not affect the limit load of the footing when the boundaries are

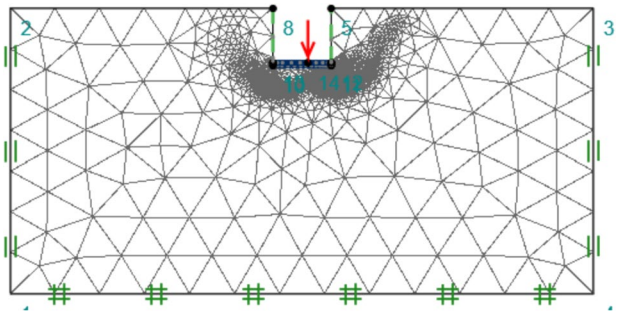

Fig. 3 Numerical model for the analysis of the bearing capacity of shallow foundations

extended further from it. All directions of the model's base are constrained. Only the horizontal direction constrains the right and left vertical sides. The soil was modeled as a linearly elastic-perfectly plastic material, obeying the Mohr–Coulomb criterion for providing Tresca material. Young's modulus increases with depth for undrained materials ($v = 0.49$, $E_u = 500\, c_u$, $\gamma = 16$ kN/m^3). The cohesion and Young's modulus of soil were assumed to vary linearly with depth z, as follows:

$$\begin{cases} c_u = c_0 + c_{\text{inc}} \cdot z \\ E_u = E_0 + E_{\text{inc}} \cdot z \end{cases} \tag{4}$$

where c_0 and E_0 are the cohesion and Young's modulus at the soil surface, respectively. C_{inc} and E_{inc} are increments of cohesion and Young's modulus per unit depth.

A rigid plate with weightless material is used to model the foundation; it is possible to determine the (V-M) capacity for another point using statics. c_0 represents the undrained shear strength at the reference point. The results regarding local soil heterogeneity $k{\cdot}D/c_0$ for a surface foundation or an infinitely thin embedded plate can be presented. An interface element defined by the Coulomb shear-strength criterion connects the rigid footing to the soil. It was always the case that the interface elements along the base of the foundation along (1) were rough (Fig. 2), and as long as the soil has a strong shear strength, the maximum shear stress can be applied. A rough interface along (2, 3) was modeled by assigning the same properties to interface elements as those along the base (Fig. 2). With a smooth interface, there was no undrained strength at the interface elements.

This study models a foundation using a weightless, rigid plate. The vertical-moment (V-M) capacity at any point can be determined using principles of statics, with c_0 representing the undrained shear strength at a reference point. The influence of local soil heterogeneity, expressed as $k{\cdot}D/c_0$, is investigated for both surface and embedded foundations. The model employs Coulomb shear-strength interface elements to connect the rigid footing to the soil. A rough interface

condition is assigned along the base of the foundation (Fig. 2), allowing for the application of maximum allowable shear stress under the assumption of undrained soil behavior. The same rough interface properties are applied to interface elements along sides (2, 3) (Fig. 2). A smooth interface is characterized by zero undrained strength at the interface elements.

Detecting the Failed Envelopes

Limit analyses are the most efficient tools for evaluating the bearing capacity of the foundation, offering a much quicker assessment than step-by-step elastoplastic analyses. The ultimate uniaxial capacities, V_{ult} ($M=0$) and M_{ult} ($V=0$), respectively, are the critical determinants for both vertical and moment directions. Bearing capacity factors are determined based on these ultimate uniaxial capacities and the undrained shear strength. The bearing capacity can be easily plotted in two-dimensional sections based on the plane (V-M), making it easier to evaluate and optimize the bearing capacity of the foundation.

Results

Comparison of Available Solutions

To accurately predict the vertical bearing capacity of a strip footing on cohesive soil under axial loading without surcharge, a numerical model was developed based on Eq. 1 Validation against Prandtl's analytical solution [25] for bearing capacity factor N_c yielded an excellent agreement, with the model's N_c value (5.18) deviating by a mere 1% from the theoretical value ($\pi+2$). This close correspondence underscores the reliability and accuracy of the implemented numerical modeling approach.

Figure 4 presents a comparative analysis of the proposed model's bearing capacity predictions with those of Edward [26], Gourvenec [27], and Salgado et al. [28]. All models demonstrate an increasing trend in bearing capacity with increasing embedment depth. Notably, our model exhibits perfect agreement with Edward's solution. Compared to Gourvenec's model, our predictions show an 18% reduction in bearing capacity while exceeding those of Salgado et al. [28] by 3.7%.

Further examination reveals nuances in the relationship between the bearing capacity factor (N_c) and the embedment ratio (D/B). The current model demonstrates a strong correlation between bearing capacity factor (N_c) and embedment ratio (D/B), consistent with Salgado et al. [28] for $D/B \le 0.5$. However, for $D/B \ge 0.5$, the model yields slightly higher N_c values compared to Salgado's lower-bound solution. Conversely, while aligning with the model for $D/B \le 1$, the

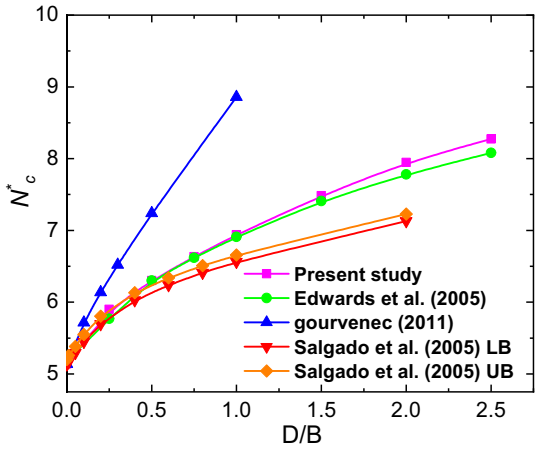

Fig. 4 Comparison between the model of the study and the model proposed in the literature

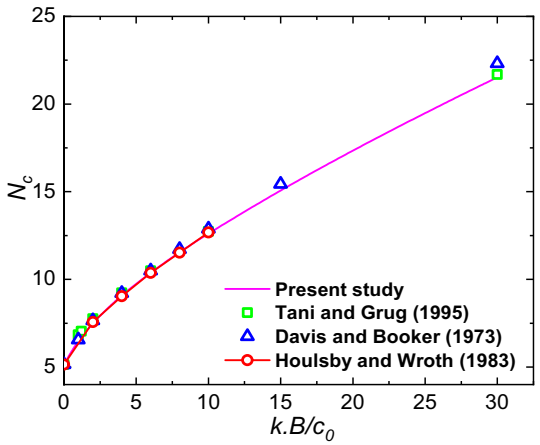

Fig. 5 Comparison of the obtained results with exact solution for the case of undrained non-homogeneous clay

solution of Edward [26] significantly underestimates N_c for $D/B \ge 1$.

Analysis of Fig. 5 reveals a significant influence of the non-homogeneity factor ($k{\cdot}B/c_0$) on the bearing capacity of embedded foundations. The model demonstrates a clear positive correlation between $k{\cdot}B/c_0$ and bearing capacity, indicating a substantial increase in bearing capacity with increasing non-homogeneity. Furthermore, an increase in $k{\cdot}B/c_0$ corresponds to a proportional rise in shear stress at the base level of the foundation. These findings align with the observations reported by Houlsby and Wroth [29]. However, while the results of Davis and Booker [30] exhibit relative similarity for $k{\cdot}B/c_0 \le 5$, they diverge significantly from the present $k{\cdot}B/c_0 \ge 5$ models, predicting higher bearing capacities.

Figure 6 presents a comparative analysis of the bearing capacity factor (N_c) under eccentric loading conditions

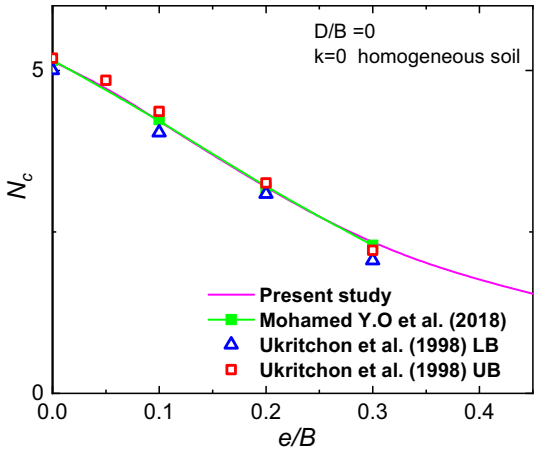

Fig. 6 Comparison of the obtained results with exact solution for the case of undrained non-homogeneous clay

(e/B) for a surface footing ($D/B = 0$) on homogeneous soil ($k = 0$). Present numerical model predictions are juxtaposed with those from previous studies. The results demonstrate a consistent linear decrease in N_c with increasing load eccentricity, aligning closely with the findings of Ouahab et al. [7]. However, discrepancies emerge when comparing the upper and lower-bound solutions of Ukritchon et al. [31]. For $e/B \leq 0.2$, their upper bound solution yields N_c values exceeding the present results by up to 0.7%, while their lower bound solution underestimates N_c by up to 0.6%. Conversely, for e/B values greater than 0.2, the present model predicts N_c values that are up to 1% higher than those obtained from the upper-bound solution of Ukritchon et al. [31]

Effect of the Footing embedment

This study comprehensively examines the undrained bearing capacity of footings at the embedment ratios (D/B) of 0 and 1. The impact of embedment and eccentric loading (e/B) on bearing capacity is also thoroughly investigated. This investigation was conducted for two separate cohesion gradients, specifically $k = 0$ and 20, and the resulting data are presented in Figs. 7 and 8, respectively.

Figure 7 (a, b) presents a comparative analysis of the normalized failure zone width (B/B_0) and its rate of reduction for a surface footing ($D/B = 0$) under eccentric loading conditions (e/B). Present numerical model predictions are compared to those obtained by Ouahab et al. [7]. Both studies demonstrate a consistent decrease in B/B with increasing e/B, ranging from 1 to 0.3. This reduction is more pronounced for non-homogeneous soil ($k = 20$) than homogeneous soil ($k = 0$).

A notable divergence between the two studies emerges beyond $e/B = 0.2$. For instance, at $e/B = 0.1$, the present model predicts V/V_{cent} values of 0.81 and 0.72 for $k = 0$ and $k = 20$, respectively, indicating a more significant influence of non-homogeneity on the failure mechanism. However, at higher eccentricities ($e/B = 0.3$ and 0.4), the V/V_{cent} values converge for both homogeneous and non-homogeneous cases, suggesting that the effect of soil non-homogeneity diminishes under significant eccentric loading.

Figure 8 (a, b) presents a comparative analysis of the normalized effective width (B/B_0) for embedded footings ($D/B = 1$) in both homogeneous ($k = 0$) and non-homogeneous ($k = 20$) clay soils. Present numerical model predictions are juxtaposed with the findings of Ouahab et al. [7] and Meyerhof's [8]. A striking agreement is observed between the present results and the effective width curves proposed by Ouahab et al. [7] and Meyerhof's [8], except for the case

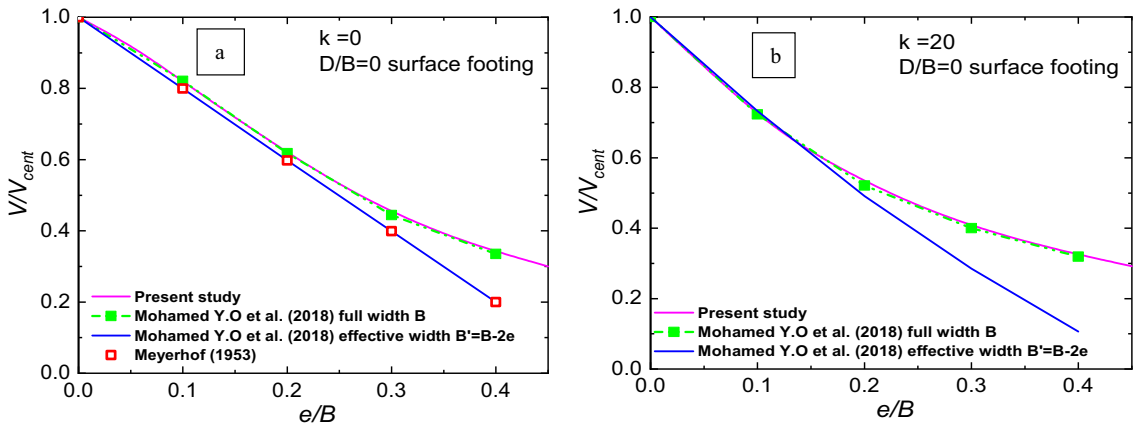

Fig. 7 Comparison of the obtained results with previous studies for the case of homogeneous and non-homogeneous clay and with embedded footing $D/B = 1$

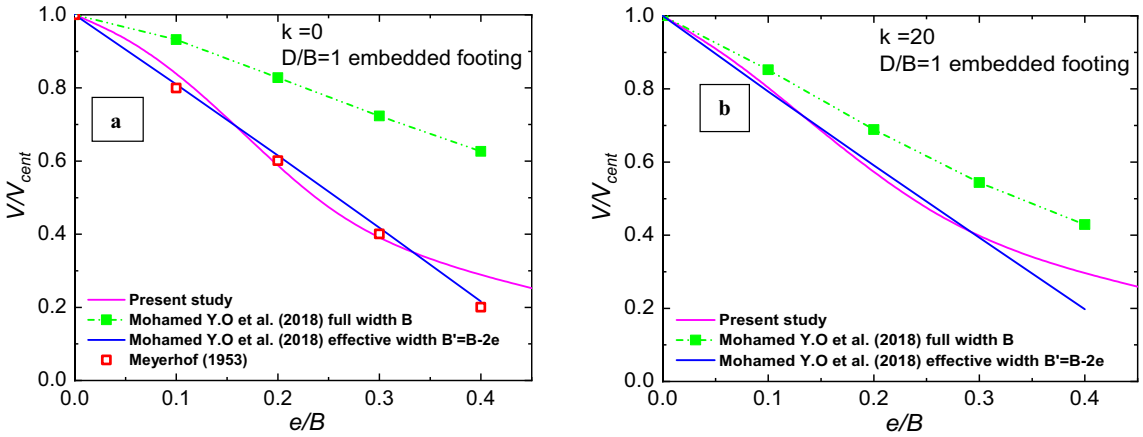

Fig. 8 Comparison of the obtained results with previous studies for the case of homogeneous and non-homogeneous clay and with embedded footing $D/B = 1$

of a surface footing ($D/B = 0$) where the full footing width is mobilized.

As anticipated, increasing load eccentricity (e/B) leads to a decrease in the normalized load (V/V_{cent}), reducing the effective width of the footing. Interestingly, the influence of eccentricity on V/V_{cent} for embedded footings appears minimal, regardless of soil non-homogeneity. For instance, at $e/B = 0.1$, V/V_{cent} values of 0.81 and 0.80 are observed for $k = 0$ and $k = 20$, respectively. Similarly, at $e/B = 0.3$, V/V_{cent} remains consistent at 0.40 for both homogeneous and non-homogeneous cases.

Effect of the interface

Figure 9 (a, b) illustrates the influence of load eccentricity (e/B), soil non-homogeneity (k), and embedment depth (D/B) on the bearing capacity of strip footings with both rough and smooth base interfaces. The analysis encompassed a range of eccentricities from 0.0 to 0.45. Notably, for homogeneous soil ($k = 0$), the bearing capacity exhibits an increasing trend with increasing eccentricity, regardless of the interface type. Conversely, for non-homogeneous soil ($k > 0$), bearing capacity decreases with increasing eccentricity for both rough and smooth interfaces. Notably, across all scenarios, rough base interfaces exhibit slightly higher bearing capacity compared to smooth interfaces.

Envelope Failure Surface

Offshore foundations are subjected to complex loading scenarios involving combined vertical, horizontal, and moment loads. Advanced geotechnical analyses often employ failure envelopes or interaction diagrams to delineate the bearing capacity limits under such combined loading. These envelopes visually represent the yield locus in a vertical-moment loading plane, enabling the assessment of foundation stability.

Figure 10 presents a normalized failure envelope (V/Bc_0–M/B^2c_0) for strip footings. Notably, the maximum moment capacity occurs under pure moment loading (zero vertical loads), suggesting full adhesion at the footing-soil interface.

For homogeneous soil ($k = 0$), the size of the yield locus expands with increasing embedment depth, indicating enhanced bearing capacity. However, in non-homogeneous soil ($k > 0$), the yield loci exhibit more complex behavior, with their size and shape varying depending on the embedment depth and the degree of non-homogeneity of soil strength. Interestingly, embedded footings ($D/B = 2$) in non-homogeneous soil demonstrate a lower moment capacity than those in homogeneous soil. As the non-homogeneity factor (k) increases, the yield loci converge, suggesting a diminishing influence of embedment depth on the failure mechanism. This variation in behavior can be attributed to the differing cohesion levels at the footing base for surface and embedded foundations, leading to distinct failure modes.

Failure Mechanism

Figures 11 shows the incremental displacements at failure for rough strip footing for various e/B ratios, namely 0, 0.1, 0.2, and 0.4. The failure mechanism consists of two symmetrical wedge zones directly beneath the footing for $e/B = 0$. This mechanism is similar to Prandtl-type failures and is symmetrical. For eccentric footing loading ($e/B = 0.1$, 0.2), the vertical and moment loading effects create the wedge and scoop zones of the failure mechanisms, respectively. When a load is applied eccentrically

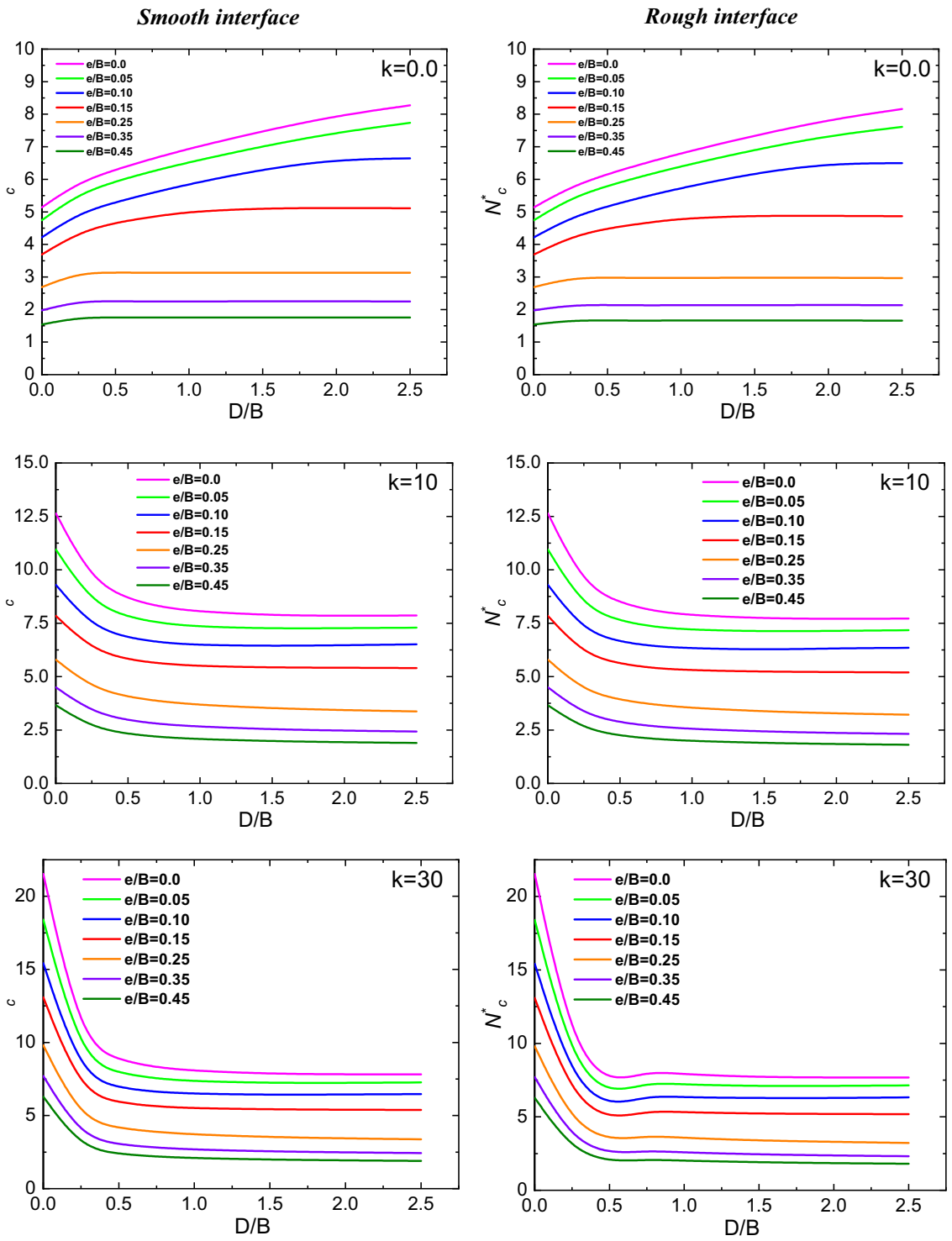

Fig. 9 The effect of *e*/*B*, *k*, *D*/*B* on the bearing capacity of rough and smooth surfaces

to a footing, stress concentrations arise in the soil near the point of load application. Consequently, the failure zones narrow as the eccentricity increases, with failure predominantly localized in the high-stress region close to the load. At an eccentricity-to-footing width ratio (*e*/*B*) of 0.4, the load is nearly at the edge of the footing. This condition triggers a distinctive failure mechanism known as the "scoop." In this mode, the soil yields along a curved or concave failure plane, excavating away from the footing edge toward the applied load.

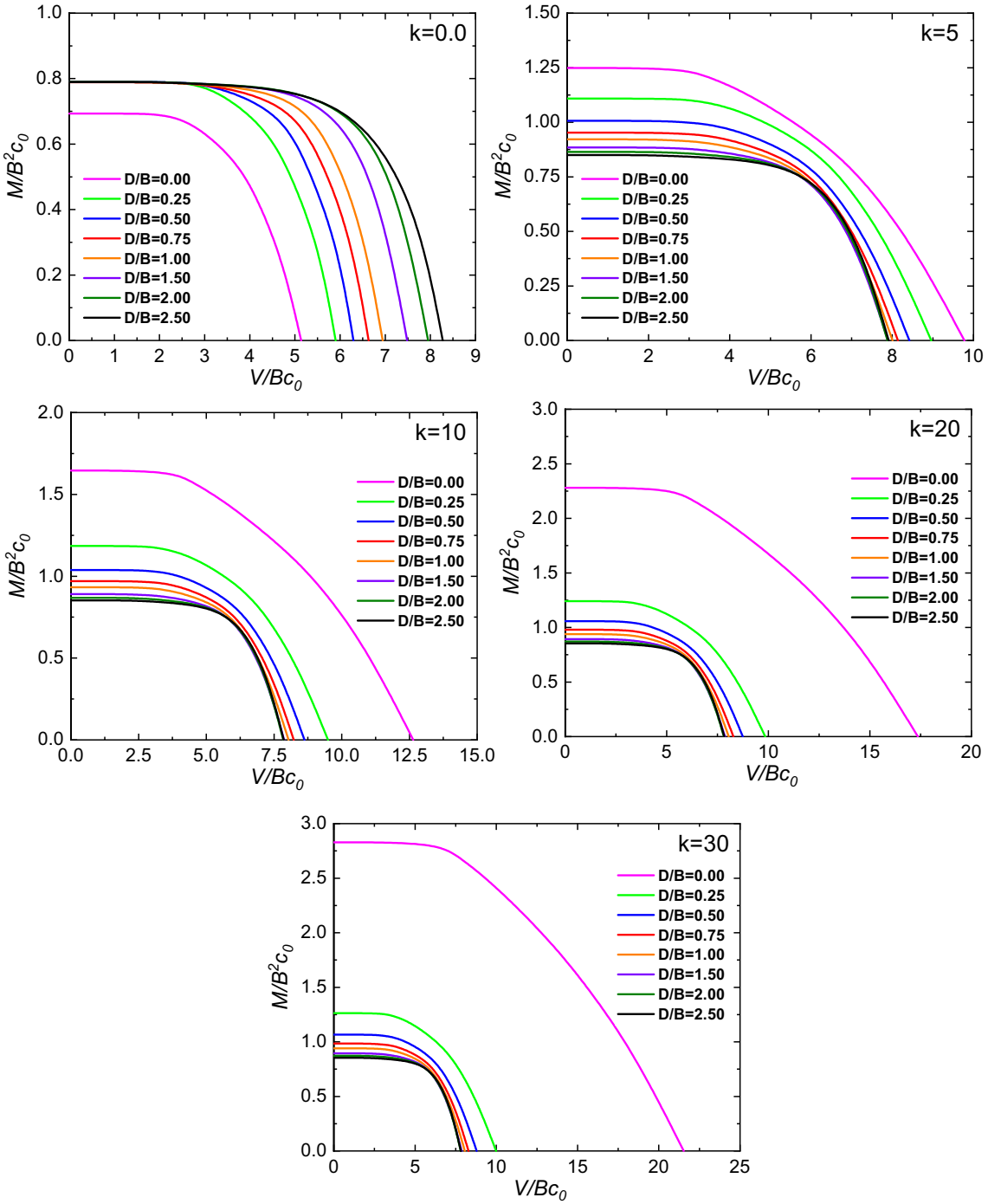

Fig. 10 Normalized failure envelopes for $k = 0$, 5, 10, 20, and 30

Conclusion

This study harnessed sophisticated numerical modeling methods to explore the bearing capacity and failure mechanisms of strip footings embedded within non-homogeneous clay soils under eccentric loading conditions. The finite element model exhibited remarkable concurrence with well-established analytical solutions, thus affirming its reliability. Through extensive parametric studies, identified significant influences of soil non-homogeneity rate (k), layer thickness-to-footing width ratio (h/B), footing embedment ratio (D/B), and load eccentricity (e/B) on both bearing capacity and failure modes.

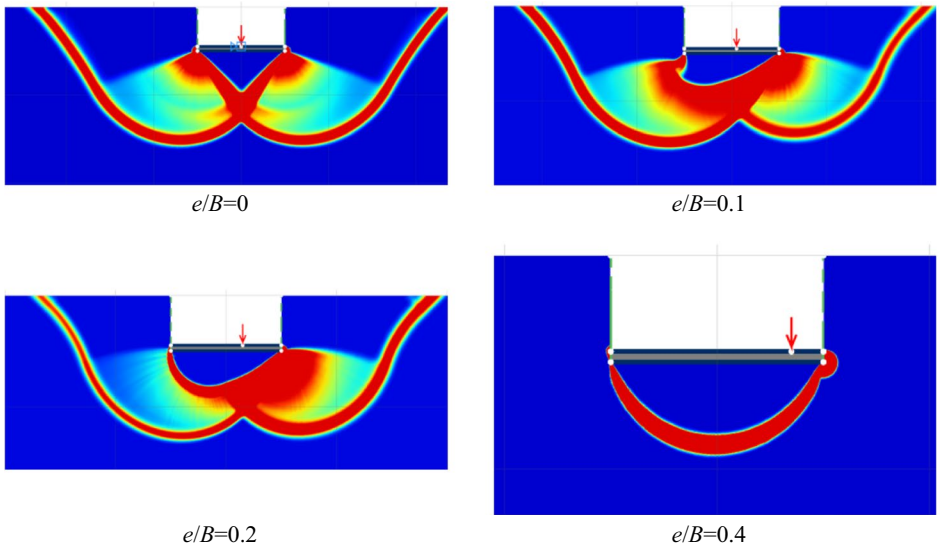

Fig. 11 Failure mechanisms for different eccentric loading *e*/*B*

The findings demonstrate that increased soil non-homogeneity (k) significantly enhances bearing capacity due to heightened shear stresses at the foundation base. Additionally, load eccentricity leads to a linear reduction in bearing capacity, particularly pronounced for surface footings compared to embedded footings. The study also elucidates the nuanced correlation between the bearing capacity factor (N_c) and embedment ratio (D/B), aligning with prior research for shallow embedments while projecting slightly elevated N_c values for deeper embedment.

Detailed failure mechanism analyses reveal the emergence of symmetrical wedge zones and localized scooping effects under eccentric loading conditions. The size and shape of yield loci within failure envelopes vary based on embedment depth, soil non-homogeneity, and interface conditions, providing valuable insights for assessing foundation stability under combined loading scenarios.

This research significantly advances our understanding of bearing capacity and failure behavior in embedded footings within non-homogeneous clays, with practical implications for geotechnical engineering foundation design.

Acknowledgements We want to acknowledge the team of LRGC Biskra.

Author Contributions Zatar Nassima acquired methodology and contributed to the investigation, data curation, and writing—original draft. BAAZOUZI Messaoud acquired software and contributed to the investigation and data curation. Alaoua Bouaicha contributed to writing—reviewing, and editing. Boudiaf Khaoula acquired software and contributed to the investigation and data curation. Zatar Abdellah contributed to writing—reviewing, and editing. Mabrouki Abdelhak contributed to reviewing and editing.

Funding This study was supported by the University of Batna and the Civil Engineering Research Laboratory LRGC, Biskra.

Data availability All data, models, or codes supporting this study's findings are available from the corresponding author upon reasonable request.

Declarations

Conflict of interest The authors declare no competing interests.

Consent for Publication Not applicable.

Ethical Approval and Consent to Participate All respondents consented to participate in the survey.

References

1. Terzaghi K (1943) Theoretical soil mechanics. Wiley, New Jersey
2. Burd H, Frydman S (1997) Bearing capacity of plane-strain footings on layered soils. Can Geotech J 34:241–253
3. Baazouzi M, Khaoula B, Mohamed T, Ouassim R, Zatar N (2023) Numerical analysis to assess the bearing capacity of footings embedded in cohesive soil slope. Transp Infrastruct Geotechno 11(1):1–20
4. Baazouzi M, Mellas M, Mabrouki A, Benmeddour D (2017) Effect of the slope on the undrained bearing capacity of shallow foundation. Int J Eng Res Afr 28:32–44
5. Randolph MF (2012) In, mechanical behaviour of soils under environmentally induced cyclic loads. Springer, Vienna, pp 441–480
6. Khitas NEH, Benmeddour D, Mellas M, Mabrouki A (2017) The undrained bearing capacity of strip footings under eccentric loading effect of soil-footing interface tensile strength. Int J Geotech Eng 14(2):169–175
7. Ouahab MY, Mabrouki A, Mellas M, Benmeddour D (2018) Effect of load eccentricity on the bearing capacity of strip footings

on non-homogenous clay overlying bedrock. Transp Infrastruct Geotechnol 5:169–186
8. Meyerhof G (1953) The bearing capacity of foundations under eccentric and inclined loads. InProc of 3rd ICSMFE 1:440–445
9. Uzuner B (1975) Centrally and eccentrically loaded strip foundations on sand, University of Strathclyde
10. Pham QN, Ohtsuka S, Isobe K, Fukumoto Y (2022) Limit load space of rigid strip footing on cohesive-frictional soil subjected to eccentrically inclined loads. Comput Geotech 151:104956
11. Bransby M, Randolph M (1998) Combined loading of skirted foundations. Géotechnique 48:637–655
12. Vulpe C, Gourvenec S, Power M (2014) A generalised failure envelope for undrained capacity of circular shallow foundations under general loading. Géotech Lett 4(187):196
13. Gourvenec S, Vulpe C, MURTHY TG (2014) A method for predicting the consolidated undrained bearing capacity of shallow foundations. Geotechnique 64:215–225
14. Bienen B, Gaudin C, Cassidy MJ, Rausch L, Purwana OA (2012) Numerical modelling of undrained capacity of hybrid skirted foundation under combined loading. Int J Offshore Polar Eng, 22(04)
15. Fu D, Gaudin C, Tian C, Bienen B, Cassidy M (2015) Effects of preloading with consolidation on undrained bearing capacity of skirted circular footings. Géotechnique 65:231–246
16. Fu D, Gaudin C, Tian Y, Cassidy MJ, Bienen B (2017) Uniaxial capacities of skirted circular foundations in clay. J Geotech Geoenviron Eng 143:04017022
17. Pham QN, Ohtsuka S, Isobe K, Fukumoto Y, Hoshina T (2019) Ultimate bearing capacity of rigid footing under eccentric vertical load. Soils Found 59:1980–1991
18. Hentati A, Selmi M, Kormi T, Ali NBH (2018) Probabilistic HM failure envelopes of strip foundations on spatially variable soil. Comput Geotech 102:66–78
19. Zheng G, Zhao J, Zhou H, Zhang T (2019) Ultimate bearing capacity of strip footings on sand overlying clay under inclined loading. Comput Geotech 106:266–273
20. Drucker DC, Prager W (1952) Soil mechanics and plastic analysis or limit design. Q Appl Math 10:157–165
21. G. Optum (2019) Optum Computational Engineering
22. Matar M, Salençon J (1979) Capacité portante des semelles filantes. Revue Française de Géotech. https://doi.org/10.1051/geotech/1979009051
23. Boudiaf K, Benmeddour D, Baazouzi M, Mabrouki A, Mellas M (2019) A numerical investigation of the effect of isotropic spatially variable tensile strength on slope stability. Transp Infrastruct Geotechnol 6:268–288
24. Brahmi N, Ouahab MY, Mabrouki A, Benmeddour D, Mellas M (2021) Probabilistic analysis of the bearing capacity of inclined loaded strip footings near cohesive slopes. Int J Geotech Eng 15(6):732–739
25. Prandtl L (1920) Uber die harte plastischer korper. Nachr. Ges. Wissensch, Gottingen, math.-phys. Klasse, 74–85
26. Edwards D, Zdravkovic L, Potts D (2005) Depth factors for undrained bearing capacity. Géotechnique 55:755–758
27. Gourvenec S, Mana DSK (2011) Undrained vertical bearing capacity factors for shallow foundations. Géotech Lett 1:101–108
28. Salgado R, Lyamin A, Sloan S, Yu H (2004) Two-and three-dimensional bearing capacity of foundations in clay. Geotechnique 54:297–306
29. Houlsby G, Wroth C (1984) Seabed mechanics. In: Denness Bruce (ed) Calculation of stresses on shallow penetrometers and footings. Springer, Dordrecht, pp 107–112
30. Davis E, Booker J (1973) The effect of increasing strength with depth on the bearing capacity of clays. Géotechnique 23:551–563
31. Ukritchon B, Whittle AJ, Sloan SW (1998) Undrained limit analyses for combined loading of strip footings on clay. J Geotechl Geoenviron Eng 124:265–276